Experiments in Fluids (2022) 63:115
https://doi.org/10.1007/s00348-022-03430-9

RESEARCH ARTICLE

Flow structure and grain motion assessments of large river widening in a physical model using ultrasonic Doppler velocity measurements

Jean-Noël Saugy[1] · Azin Amini[1] · Giovanni De Cesare[1]

Received: 2 November 2021 / Revised: 29 March 2022 / Accepted: 6 April 2022 / Published online: 7 July 2022
© The Author(s) 2022

Abstract

Local river widening aims to reduce the flood risk and enable the self-morphodynamic development of the river. However, a large amount of transported sediments settles due to the flow velocity reduction in the widening. Assessing the flow and the grain motion is therefore a key factor to the sustainability of a local river widening project. The grain motion depends on the ratio between tractive forces and resisting forces, which can be evaluated through the local shear stress. The most common method to estimate shear stress in uniform flows is to determine the shear velocity based on the logarithmic distribution of velocity over depth. This involves knowing the velocity profile and in turn the flow structure. In the present study, morphodynamic tests are conducted to explore the hydrodynamics and the grain motion of a local river widening in the framework of the 3rd correction of the Rhone River, the largest flood protection project in Switzerland so far. The ultrasonic velocity profiler method is used to measure velocity profiles at two selected cross-sections. The obtained velocity profiles allow for the assessment of local shear stress on the mobile riverbed. The results show a non-uniform distribution of the flow and the shear stresses. The flow conditions at the preferential channel are more favorable to grain motion compared to those at the river's edges.

✉ Jean-Noël Saugy
jean-noel.saugy@epfl.ch

[1] Platform of Hydraulic Constructions, Ecole Polytechnique Fédérale de Lausanne (EPFL), Station 18, 1015 Lausanne, Switzerland

Graphical abstract

1 Introduction

1.1 River widening

Local river widening has become a mainstream approach to river management. It aims to reduce flood risk, and enable the self-morphodynamic development of the river (Formann et al. 2007; Berchtold et al. 2012), increasing its ecological potential (Eawag et al. 2005; Rohde et al. 2005; Weber et al. 2009; Schirmer et al. 2014). During early morphological studies regarding large river widenings, an increase in the mean bed elevation has been taken into account relative to the upstream and downstream channelized sections (Hunzinger 1998), a large amount of transported sediments would settle there due to the reduced flow velocity. Factors such as a poor design and/or a lack of sediment extraction can partially or fully inhibit the widening and its function. Assessing the flow and bedload processes in a large river widening is a key factor in understanding the sustainability of the project.

The 3rd Rhone River training work is the largest flood protection project in Switzerland (Canton of Valais 2015). A total of 140 km of the river will be widened, including several large and complex widenings (Jenzer et al. 2008). Approaching the town of Martigny, the Rhone River forms a nearly 90° bend, which has leads to large damages upstream related to flooding, according to the region's hydraulic hazards map (Canton of Valais 2020a, b). Therefore, this section was set as a priority area. It is planned to lower and widen the Rhone River bed as well as to create a large river widening between a upstream block ramp and the downstream bend, hereafter referred to as the Verney widening. The upstream bedload transport is estimated to be approximately 30,000 m^3 per year without extractions (Essyad et al. 2014). Therefore, the grain behavior in the widened area must be assessed to avoid filling.

1.2 Sediment motion

The motion of grain particles depends on the ratio between tractive (shear) and restrictive (inertia, friction) forces (Shields 1936). When internal forces are stronger than hydrodynamic forces, particles cannot be transported by the river. If the tractive forces exceed the gravitational forces, then particles will be dislodged and start moving. This process is thus subject to a threshold, which has been studied by different approaches but

always consists of a separation curve between motion and no motion (Hjulström 1935; Inman 1949; Lane 1955; Sundborg 1956).

The most common approach was proposed by Shields (Shields 1936). He linked the incipient motion with "a critical ratio of the applied bottom shear stress to the immersed weight of the grains" (Paphitis 2001), i.e., the Shields parameter (θ_{cr}). His dimensionless ratio can be expressed as:

$$\theta_{cr} = \frac{\tau_{cr}}{(\rho_s - \rho)gd} \tag{1}$$

where τ_{cr} corresponds to the critical bed shear stress, g corresponds to the gravitational force equivalent, ρ_s and ρ correspond to the sediment and fluid densities, respectively, and d corresponds to the grain diameter. Shield's results showed a relation between his parameter and the granular Reynolds number (Eq. 2) as well as a curved narrow band threshold divided into four specific regions.

$$\mathrm{Re}_* = u_* \mathrm{d}/\nu \tag{2}$$

where ν is the kinematic viscosity and u_* is the shear stress velocity. The latter parameter is calculated as follows:

$$u_* = \sqrt{\tau/\rho} \tag{3}$$

where τ corresponds to shear stress. Shear stress is a property of the flow while critical shear stress is a property of the grains. As shown in the previous equations, shear stress is a key parameter for determining grain motion. If τ exceeds τ_{cr}, then θ will be higher than θ_{cr}. In this case, flow conditions overcome the resistance of the bed and grains will move.

Direct optical approaches have been applied to monitor inception of sediment motion, and bedload transport (Pilotti et al. 1997; Radice et al. 2006; Bohling 2009; Tal et al. 2012). However, they involve visual observations of the environment and require rather clear water and a flume setup. Several indirect methods have also been proposed (Biron et al. 2004), that aim to assess grain motion by estimating shear stress. The most common estimation methods use local velocity measurements to determine u_* (depth-averaged velocity in the vertically averaged logarithmic velocity profile, single near-bed velocity observations, and slope of the near-bed velocity profile) (Wilcock 1996). Indeed, a logarithmic function exists between the shear velocity and the variation of velocity with height (Eq. 4) (Schlichting et al. 1979).

$$\frac{u}{u_*} = \frac{1}{\kappa} * \ln\left(\frac{z}{z_0}\right) \tag{4}$$

where κ corresponds to von Kármán's constant (Von Kármán 1930), u corresponds to the mean longitudinal velocity at height z above the bed, and z_0 corresponds to the height at which the mean velocity is equal to zero (Worley 1972). According to flume experiments on flows with bed-load transport (Gaudio et al. 2010a, b), Von Kármán's constant lies between 0.3 and 0.4; therefore an average value of 0.35 has been applied.

In addition to computing high values of bed shear stress in a simple boundary layer (Biron et al. 2004), this method can only be used in a noncomplex flow field to ensure a logarithmic region (Duma et al. 2014). According to Bagherimiyab and Lemmin (2013), the top limit of the log layer corresponds to 0.2 h (h = flow depth). However, the logarithmic profile reestablishes quickly after disruption (Meile et al. 2008). The velocity profile must be known to apply this method, meaning that the flow structure must be determined.

1.3 Velocimetry

In hydraulic research, velocimetry techniques are numerous, e.g., particle image velocimeters (PIV) (Muste et al. 1998), pitot tubes, electromagnetic velocimeters, propellers, hot wires, hot films, laser Doppler velocimeters (LDV) (Muste et al. 1998), laser Doppler anemometers (Biron et al. 1996), acoustic Doppler velocimeters (ADV) (Wang et al. 2012), and ultrasonic velocity profiling (UVP) (Yamanaka et al. 2002). Some of these techniques depend on visibility, e.g., LDV, and PIV. As previously explained, optical instruments work well in rather clear fluids with large particles. Moreover, the instrument location is often above or on the side of the flume. In addition, some methods need a turbid environment to work, e.g., LDV, ADV, and UVP.

UVP can measure an instantaneous velocity profile of river flow along a measurement line, using Doppler-shifted frequency in echoes reflected by transported sediments (Takeda 1986, 1991). In the field of hydraulics, some of its applications are characterization of flow (Hersberger 2002; Rosier et al. 2004; Kantoush et al. 2008), and/or bed morphology evolution (Rosier et al. 2004; Guney et al. 2013). Nevertheless, post-processing can be applied to reveal more phenomena, e.g., the stability of gravel beds (Duma et al. 2014).

The objective of the present paper is to determine and show how measured velocity profiles using ultrasonic velocity profiling can improve the estimation of bedload motion in a large-scale experiment with a complex geometry. The limits of the selected approach are as well considered.

2 Experimental setup

2.1 Study perimeter

The "Martigny bend" measure covers the perimeter between kilometers 39.7 and 35.0, although only the main segment between kilometers − 9.7 and 37.1 is physically modeled

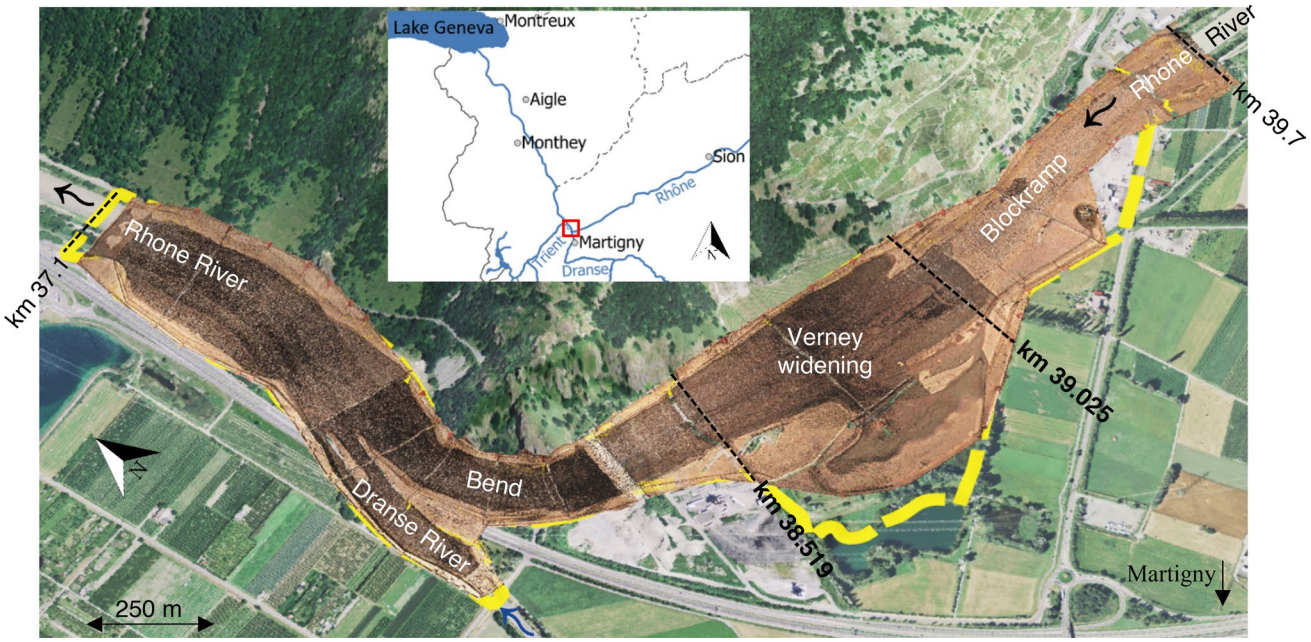

Fig. 1 Physical model perimeter (yellow line) and scaled cloud point at its initial state (orthophotos from Swisstopo)

Table 1 Scaling ratios based on Froude similarity

Parameter	Scaling ratio
Length	$\lambda = 52$
Velocity/time	$\lambda^{1/2} = 7.21$
Discharge	$\lambda^{5/2} = 19'499$
Roughness	$\lambda^{-1/6} = 0.52$

Table 2 Grain size of the transported sediments and the riverbed sediments of the widening

	Prototype scale (mm)	Model scale (mm)
d_{25}	26	0.5
d_{m}	43	0.8
d_{90}	86	1.6

(Fig. 1). The widening area (km 39.025–38.519) is located upstream of the Rhone River bend. It is 675 m long and between 90 and 100 m wide at the base of the banks. Its width can reach 200 m including the berms, while the current channelized Rhone River width is less than 50 m.

2.2 Similarities

The Rhone River hydraulic model respects the conditions of Froude similarity (Yalin 1971). The Froude number is thus the same at prototype and model scales. By respecting this similarity, all the scaling ratios can be related to one unique ratio, the geometrical scaling ratio (λ). Based on the perimeter to be modeled, and the available space for the model, the length ratio was fixed at 1:52. Therefore, time, velocity, discharge, and roughness scale factors are determined (Table 1). A noncohesive sand (Table 2) was used

Table 3 Morphodynamic scenarios tested on the physical model (Source of data: Groupement du Coude du Rhone)

	Discharge				Solid discharge			
	Rhone river		Dranse river		Rhone river		Dranse river	
	Prototype scale (m^3/s)	Model scale (l/s)	Prototype scale (m^3/s)	Model scale (l/s)	Prototype scale (kg/s)	Model scale (g/s)	Prototype scale (kg/s)	Model scale (g/s)
Q10	669	34.3	95	4.9	80	3.4	64	2.7
Q50	885	45.4	99	5.1	113	4.8	70	3.0
Q100	**1260**	**64.6**	**144**	**7.4**	**169**	**7.2**	**152**	**6.6**
Extreme flood	1600	82.1	204	10.5	220	9.3	310	13.4

Bold values are tested during this research project

for simulating bedload transport. Prior to the tests, sediment motion at prototype and model scales was compared in the Verney widening. The results were close to the ones of the Lavey Run-of-River hydropower plant project (Bieri et al. 2012) due to the project proximity.

2.3 Scenarios

Two main sets of experiments are carried out: clear water tests and morphodynamic tests. Morphodynamic scenarios with a movable bed and sediment transport, aim to recognize the erosion/deposition zones and evaluate the sediment transport capacity of the future Rhone and Dranse rivers, especially at their confluence zone as well as the upstream part of the bend. For the Verney widening, the bed grain size distribution corresponds to the transported sediment. The tested scenarios are presented in Table 3. All tests are conducted under steady-state conditions with a constant discharge corresponding to the flood peak. The present paper discusses only the results recorded during a simulation of a 100-year return period flood event (flood event with 1% probability of being equaled or exceeded in any given year).

2.4 Initiated morphology

Prior to the measurement campaign with UVP (simulation of a 100-year Rhone River flood event), morphodynamic tests (with mobile bed and sediment feeding) with lower discharges were performed as shown in Table 3. As shown in Fig. 2, a specific morphology appeared in the Verney widening. An elongated deposit formed along the initial alluvial terraces partially covering them. This deposit consisted of a succession of asymmetrical dunes. From its left limit to the Rhone River left bank, a smooth and large bed covered by asymmetrical ripples formed. This part will be referred to as the preferential channel. This asymmetry shows that currents are mainly unidirectional and steady (Best 2005). This observation confirms the initial assumption of subcritical flow.

2.5 Instrumentation

Flow velocities in the Verney widening are investigated using the UVP-DUO instrument from Met-Flow (Switzerland). This method has been applied in several research projects at The Platform of Hydraulic Constructions (PL-LCH) of the Ecole Polytechnique Fédérale de Lausanne (EPFL) since 1995 (De Cesare and Boillat 2006). These projects include interface detection between two-phase fluid (Amini et al. 2009), and mining pit development (Nilipour et al. 2004).

Two ultrasonic velocity profiler transducers are installed on a mobile support for assessing both streamwise and crosswise velocities (Fig. 3). The 2 MHz transducer beams cross at a depth of 70 mm (model scale) and have a $15° \pm 3°$ wave incidence angle to normal (θ). They are manually activated to avoid cross noise (Metflow 2002). The ultrasonic probe tip must be fully immersed in water, which reduces the recording window except for the first recordable channel along the beam axis (4.07 mm). The UVP precision is 2.342 mm/s at the model scale. The probe support is moved along two existing rails at km 39.025 and 38.519 (boundaries of the widening). No velocity data could have been recorded

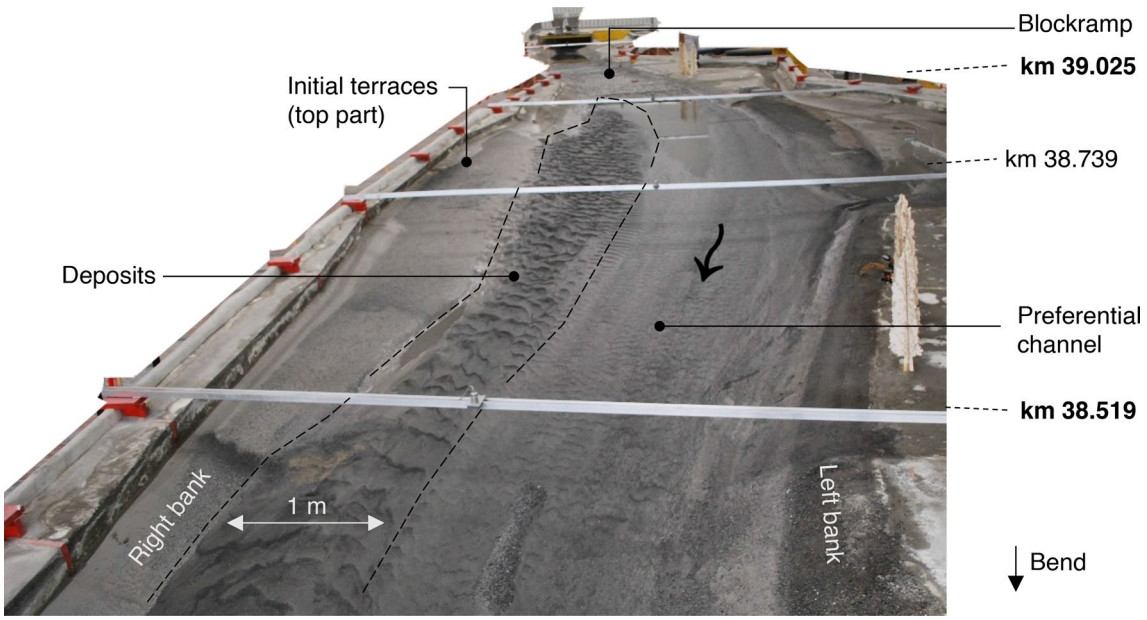

Fig. 2 Verney widening in the physical model after morphodynamic

Table 4 UVP transducer parameters

Parameter	Value	Unit
Cycle number	8	–
Repetition number	256	–
Number of profiles	100	–
Sampling rate	6.3	Hz
Voltage	60	V
Gain	3–6	–
Start point	4.07	mm
Channel distance	2.96	mm
End point	149.11	mm
Number of channels	50	-
Maximum depth	456.58	mm
Maximum velocity	±297.5	mm/s
Velocity resolution	2.342	mm/s
PRF	1.62075	kHz

elsewhere because of the required rail and the model width in the studied section. For each cross-section, the distance between two velocity profile measurements is equal to 0.1 m at the model scale (Fig. 5 [A4]). However, in some specific cases (presence of ultrasonic limnimeters, banks, etc.), this distance must be adapted. Each transducer station consists of 100 velocity records based on the ultrasonic parameters listed in Table 4. While the UVP method allows for the measurement of a velocity profile (Fig. 5 [A1]), the signal echo can also be recorded to detect the riverbed (Fig. 5 [A6]).

As previously explained, the starting point of the recording window does not correspond to the water surface. To check the discharge by calculating the integral of the stream velocity over the cross-sectional area of the flow, one ultrasonic limnimeter (US) per cross-section records the water surface elevation (WSE) before and after the UVP measurements (Figs. 3, 4 [A2]). The limnimeter precision is 1 mm at the model scale.

Although the riverbed can be detected with the UVP echo signal, detection occurs only along the beam axis. And, the cross-sections have complex bedforms. To extend the velocity profiles, the riverbed must be characterized along the cross-section. A lidar survey is therefore carried out with a ScanStation P20 from Leica (Switzerland) mounted head-down on a crane [A3]. With a wavelength of approximately 808 µm, the lidar beam can pass through water and thus detect the riverbed (Hinkelammert et al. 2016). However, water turbidity is usually too high. As a result, lidar surveys are carried out under dry conditions with an empty model, which occurs at the end of the test, just after the UVP measurements are performed (Franzetti et al. 1982). It is assumed that the bathymetry does change between the time of UVP measurements to the collection of the lidar survey. The P20 precision is 3 mm at the model scale.

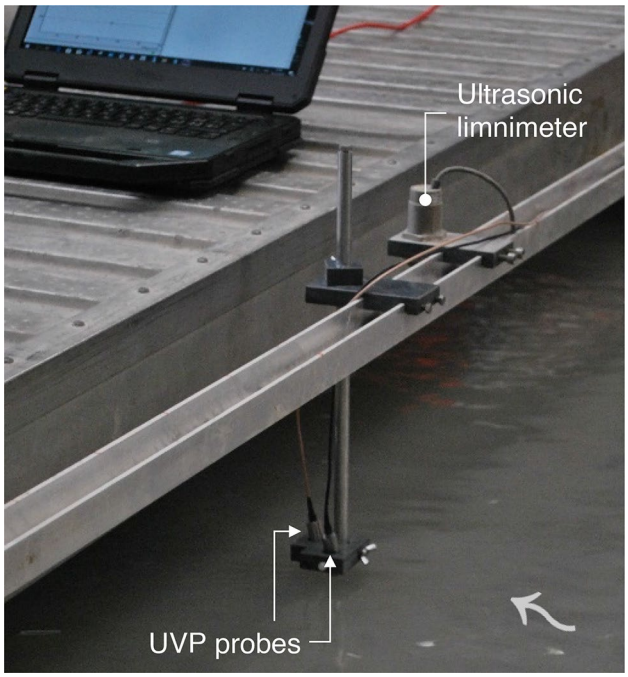

Fig. 3 Ultrasonic velocimetry profiling probe and ultrasonic limnimeter setup on the rail at km 38.519

3 Data processing

Data post-processing is summarized in Fig. 4. In addition to the acquisition [A], data post-processing is divided into three phases: preprocessing [B], flow structure assessment [C], and shear stress prediction [D]. The early phase consists of cleaning and transforming all data at prototype scale to merge the information for the next phases [B]. UVP records only the velocity component along the beam axis [B1]. By correcting it with the wave incidence angle to normal (Eq. 5), the velocity profile along the section plan can be obtained.

$$v = \frac{v_{\mathrm{UVP}}}{\sin(\theta)} \tag{5}$$

where v is the assumed horizontal velocity (stream or cross-wise) and v_{UVP} is the velocity acquired with UVP along the measurement line.

Distance and velocity values are scaled according to the scale factors [B2]. The time-averaged velocity profile and the standard deviation are then calculated [B3] as well as the echo signal derivative [B4]. The riverbed channel corresponds to the derivative local extremum, and the US

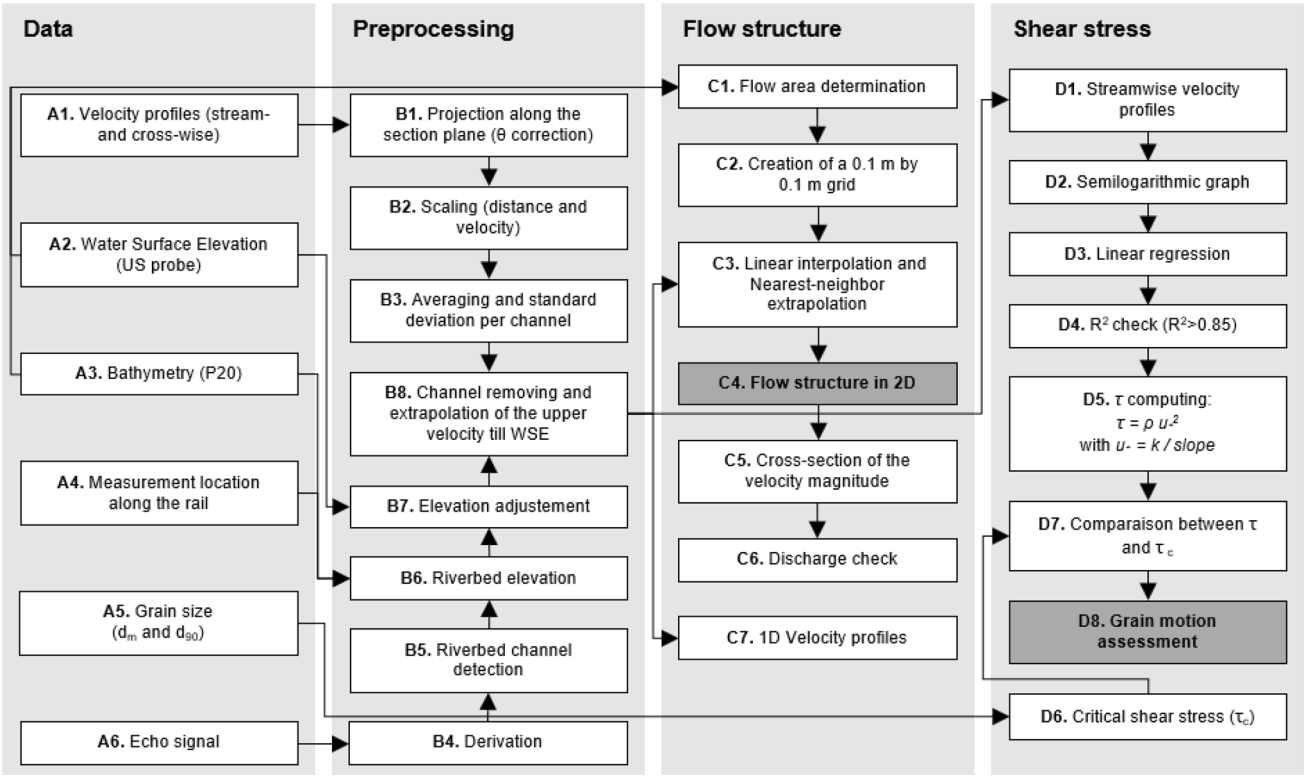

Fig. 4 UVP data post-processing steps

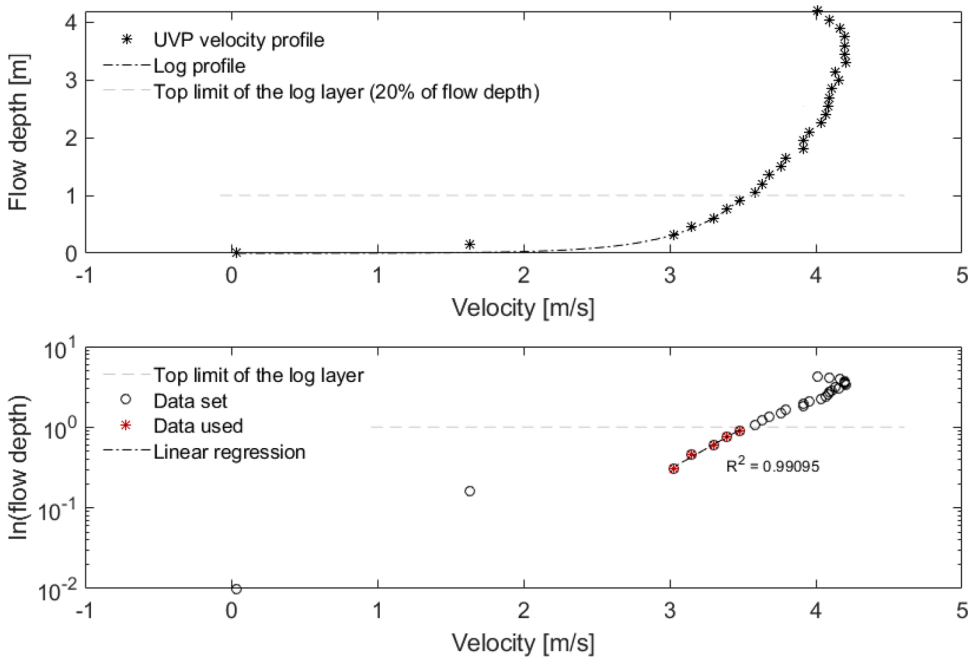

Fig. 5 Example of linear regression on the semi-log profile of the mean UVP velocity profile of the measurement N°20 for the cross-section at km 38.519

reflection is at its peak. The maximum detection error is equal to the channel width in the section plan (2.86 mm). After determining the riverbed elevation of the corresponding UVP channel [B6], all the distances to the probes are adjusted in elevation [B7]. For B6, it is assumed that the bathymetry gradient is low between the section plan and the intersection point between the measurement line and the riverbed. The last step of the preprocessing phase consists

of removing the channels strongly influenced by the probe proximity, i.e., the first three channels in general, and extrapolating the velocity of the remaining top channel until reaching the WSE [B8]. This process was not performed for the standard deviation results.

The next phase [C] is to assess the flow structure in 1D [C7] and 2D [C1-C6]. First, the flow area is determined by assuming a planar WSE [C1]. Velocity data are linearly interpolated between velocity profiles and extrapolated based on the nearest neighbor [C3] on a 0.1 m × 0.1 m grid [C2]. This resolution was selected as a standard value. The results are plotted for each cross-section and each direction (C4). The velocity magnitude is calculated for each grid cell according to the velocity projection on an assumed horizontal velocity vector [C5]. The z component is assumed to be negligible. The discharge is thus estimated thanks to the integral [C6]. For both cross-sections, the integral discharge was less than 10% of the one applied.

The last phase [D] aims to assess the grain motion by computing the shear stress based on each individual streamwise velocity profile [D1-D5] and comparing it to the critical shear stress [D6-D8]. This allows for an analysis of the contribution of turbulent fluctuations with a frequency lower than the sampling rate (3.6 Hz). A regression of the velocity on *lnz* in the log layer was applied (Bagherimiyab and Lemmin 2013) (Fig. 5). The channel window where the fitting occurs can be manually adjusted for improvement, especially at the bottom part. The profiles with a coefficient of determination (R^2) lower than 0.85 are ignored in the later steps [D4]. Equation 3 and 4 are transformed and applied to calculate the shear stress [D5]. According to Shields (Shields 1936), the critical shear stress is a function of the dimensionless critical shear stress (θ_{cr}) and grain size (d) (Table 2). Only d_m and d_{90} are used (Table 2), and θ_{cr} in the Shields region IV is equal to 0.055 (Van Rijn 1984).

$$\tau_{cr} = \theta_{cr} * \rho * g * (s-1) * d \tag{6}$$

where s is the ratio between the sediment and fluid densities.

P20 data must be processed before use in steps B6 and C1. Indeed, it acquires a point cloud in a coordinate system centered on the laser transmitter. Because of its location above the model (no access), P20 could not be leveled, and therefore, its own tilt affected the data. To correct this issue, the coordinate system is changed to a local system determined by a surveying company and based on a processing integrated into Cyclone software developed by Leica. The aligned point cloud is then cut according to the model perimeter and cleaned around the rail shadow. After this step, the coordinate system is once again changed, with the tool Absolute Orientation (Matt 2021) based on Horn's method (Horn and Schunck 1981) used to georeference data in the CH1903 + MN95 coordinate system (prototype scale). Finally, the bathymetry of the cross-sections was extracted.

4 Experimental results

Once analyzed, the UVP results are used to study the flow hydrodynamic characteristics, i.e., velocity profiles and variations as well as bed shear stresses.

4.1 UVP velocity profiles

1D averaged velocity profiles show some spatial trends along the cross-sections. Streamwise, the velocity profiles acquired in the preferential channel (Figs. 6, 7) show the highest velocities for each cross-section (Figs. 8, 9). The values are between 2.5 and 4 m/s. The profiles in the preferential channel are logarithmic with a strong near-bed gradient. Conversely, the velocity profiles on the sides of the channel tend to be less logarithmic and have lower velocities. The flow structure seems to be similar between the two cross-sections. For the cross-section at km 38.519, there is a secondary channel between 30 and 50 m (from 3 to 6).

Crosswise, the results highlight inverse trends between the two cross-sections, although the two velocity profile groups observed streamwise can still be distinguished

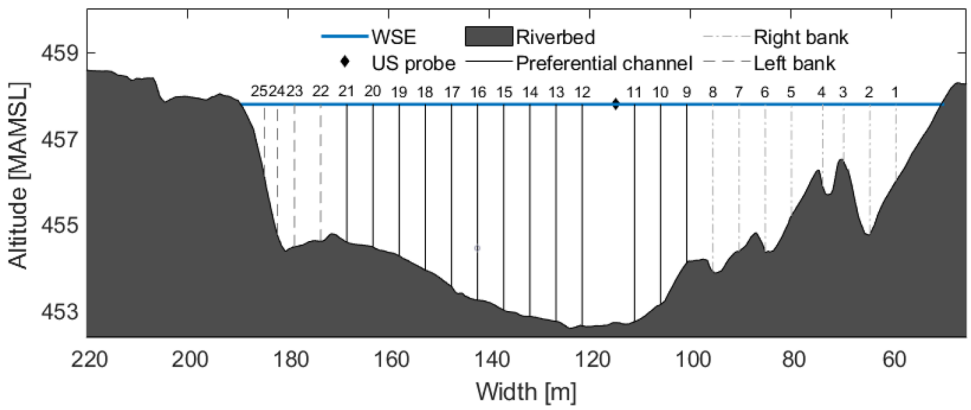

Fig. 6 UVP measurement locations for the cross-section at km 39.025

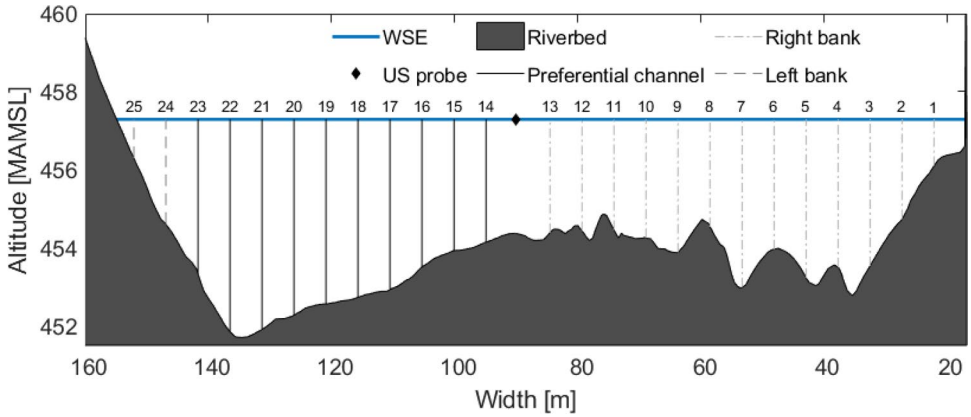

Fig. 7 UVP measurement locations for the cross-section at km 38.519

(Figs. 10, 11). For the cross-section at km 39.025, the velocity values in the preferential channel are mainly negative, meaning a flow orientated to the left bank, while the velocity vector on the left bank tends to be oriented to the left. For the cross-section at km 38.519, the velocities in the preferential channel are between -0.5 and 0. The flow seems to be slightly oriented to the right. They are more scattered than those for the previous profile. This is also the case for the left and right bank velocity profiles. Moreover, the profiles are less smooth. The crossflow at km 38.519 seems to be more affected by the section and widening geometries (Figs. 9, 10, 11).

4.2 Statistics of velocity variation

A flow is not only characterized by its streamwise and crosswise velocity components, but also by variations of these latter in space and time. High variations mean areas of complex flows. However, the method applied in the present paper is strongly affected by complex flows.

As a first step, the variation rates between velocity magnitude and streamwise velocity are studied. The variation rates between the averaged velocity magnitude and the averaged streamwise velocity for both transects are near 0, meaning that the streamwise velocity is close to the velocity magnitude (Fig. 12). The crosswise is thus mostly nonsignificant except for some specific parts above the right deposits. Their variation rate is higher than 0.2, and the crossflow component is thus not negligible.

Moreover, standard deviation for crosswise and streamwise velocities are derived and presented in Figs. 13 and 14 in order to assess the temporal evolution of flow. The standard-deviation results are like the previous results and independent of the flow assessment direction. Lower standard-deviation area can be found in the preferential channel compared to those for the sides, especially above the dunes for both cross-sections. The velocities are more dispersed.

4.3 Bed shear stress

In order to evaluate the flow capacity to move sediments, bed shear stresses are considered. Results are shown in Figs. 15 and 16. Note that the bed shear stress is only calculated if R^2 is greater than 0.85. At the km 39.025 cross-section, the shear stresses are mainly lower than $\tau_{cr,dm}$. However, within and near the preferential channel, the values mostly ranged between $\tau_{cr,dm}$ and $\tau_{cr,d90}$. The calculated shear stress exceeded $\tau_{cr,d90}$ only for the profile at 111 m. For the cross-section at km 38.519, there are three profiles in this case: two in the preferential channel and one at 80 m. In fact, the

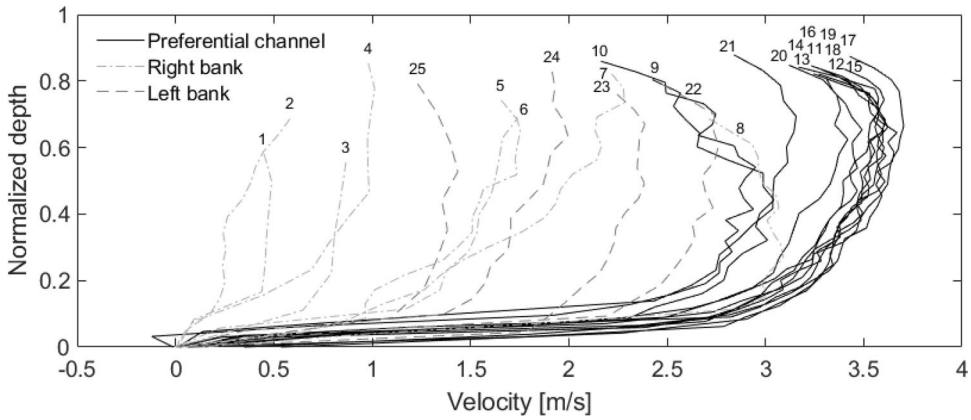

Fig. 8 Averaged streamwise velocity profiles along the normalized depth for the cross-section at km 39.025

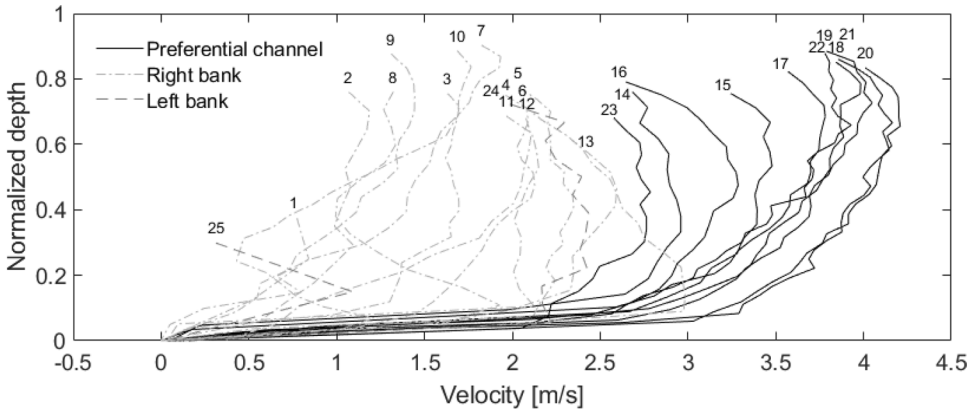

Fig. 9 Averaged streamwise velocity profiles along the normalized depth for the cross-section at km 38.519

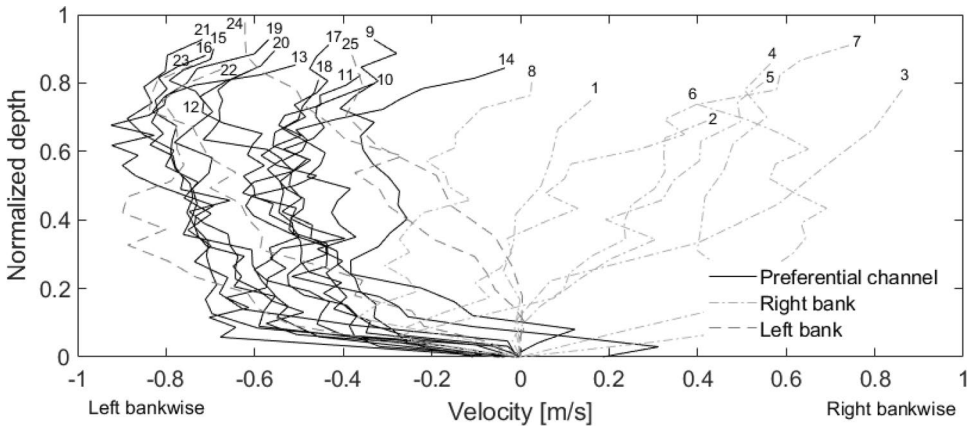

Fig. 10 Averaged crosswise velocity profiles along the normalized depth for the cross-section at km 39.025

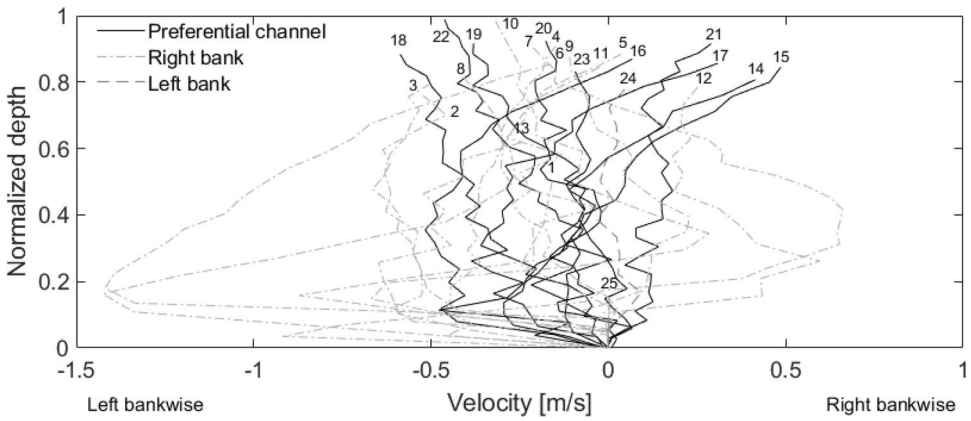

Fig. 11 Averaged crosswise velocity profiles along the normalized depth for the cross-section at km 38.519

shear stress in the preferential channel always exceeds $\tau_{cr,dm}$. Above the deposits, the shear stress is not calculated for six-velocity profiles, whereas for the upstream transect, the shear stress is not calculated for only three profiles. Moreover, the values are widely spread except for those of the right bank.

5 Discussion

5.1 A structured flow

All the previously presented results have similar patterns. The flow is structured in two parts following the bathymetry. Above the deepest part of the two transects, high velocities that show low dispersion and mainly occur in the flow

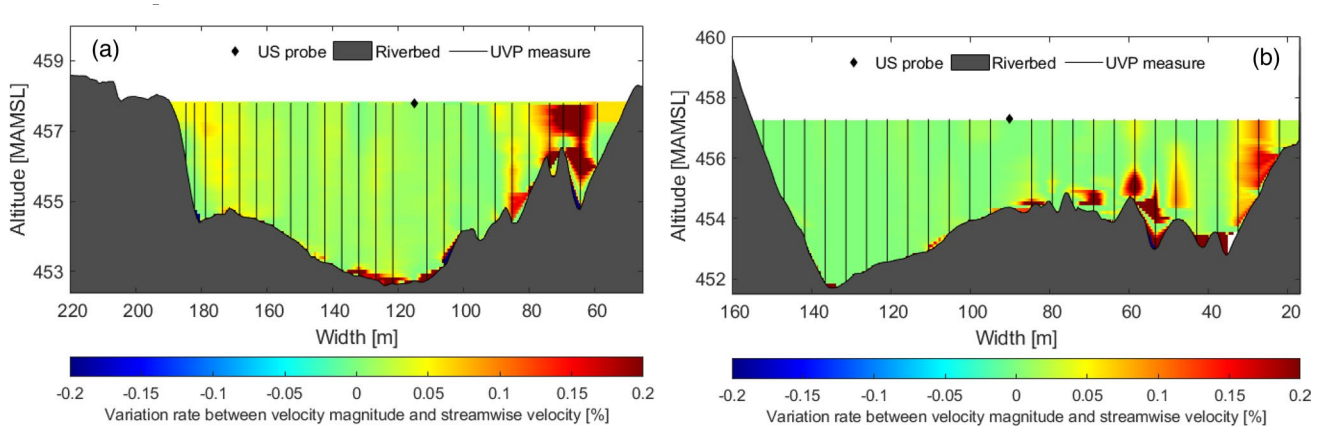

Fig. 12 Variation rate between the averaged velocity magnitude and the averaged streamwise velocity for the cross-sections at km 39.025 (**a**) and km 38.519 (**b**)

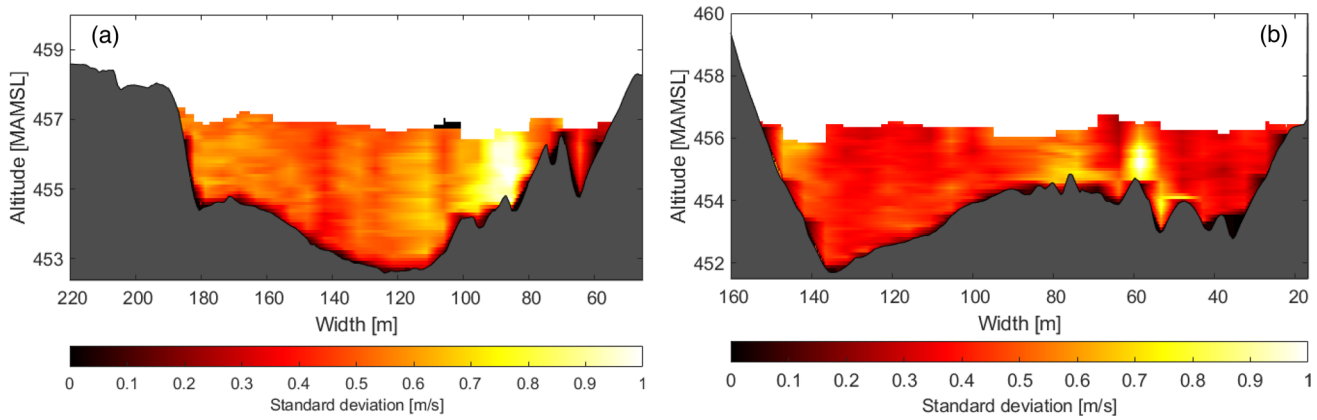

Fig. 13 Streamwise and crosswise velocity standard deviations for the cross-sections at km 39.025 (**a**) and 38.519 (**b**)

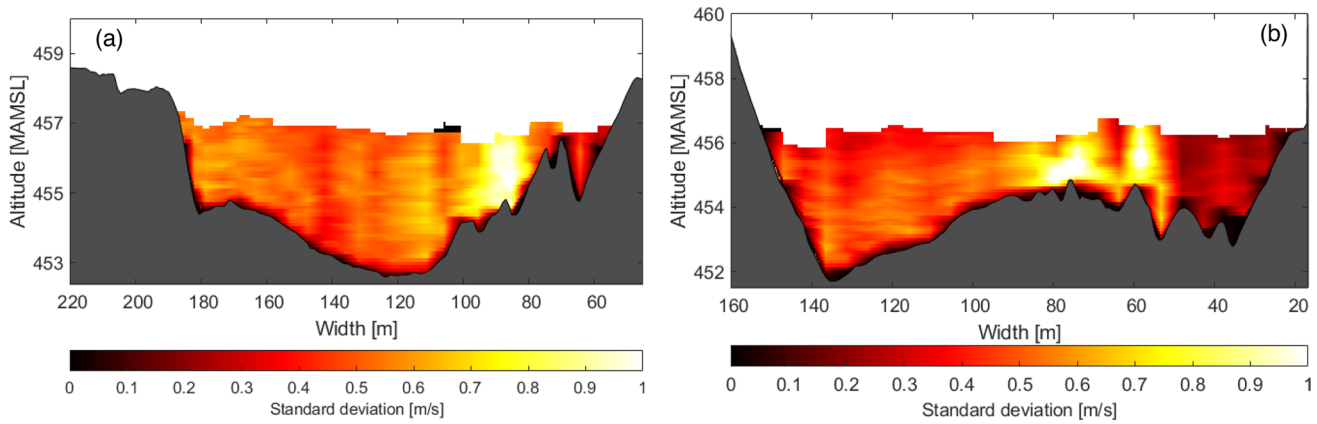

Fig. 14 Crosswise velocity standard deviations for the cross-sections at km 39.025 (**a**) and 38.519 (**b**)

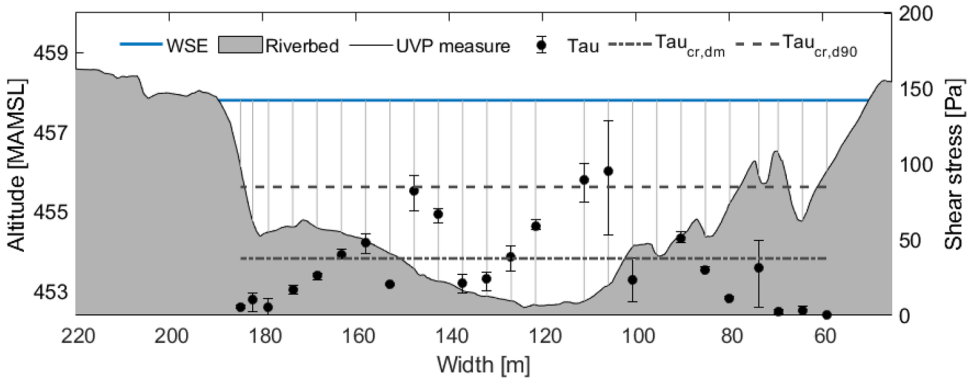

Fig. 15 Bed shear stresses estimated on the velocity log profile for the km 39.025 cross-section and critical shear stresses for d_m and d_{90}

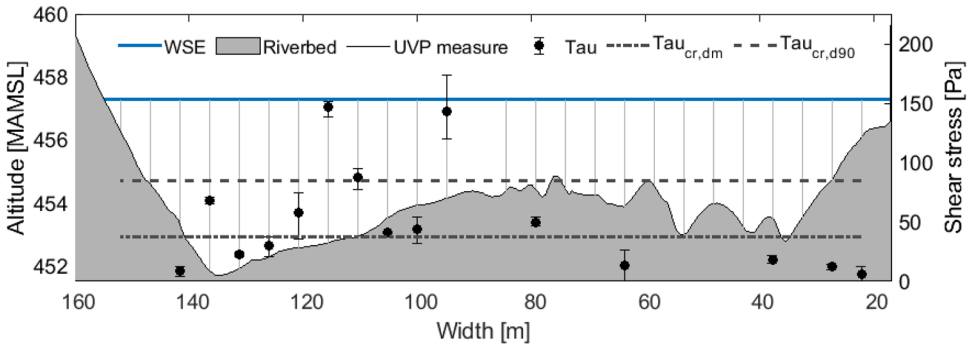

Fig. 16 Bed shear stresses estimated on the velocity log profile for the km 38.519 cross-section and critical shear stresses for d_m and d_{90}

direction have been measured streamwise and crosswise, while low velocities that show high dispersion and are influenced by the crossflow have been observed above the deposits.

The inter-transect differences, especially in the crosswise direction, can be explained by their location and the upstream or downstream conditions. For example, the crossflow after 90 m at km 39.025 is mainly oriented toward the left bank because of the upstream block ramp. This effect has already been observed for purely hydraulic tests. The crossflow is oriented toward the right because of a recirculation at the end of the block ramp. Conversely, the Verney downstream part is influenced by the Rhone River bend. Indeed, its cross-section narrows from km 38.739 (maximal width: 100 m) to km 38.113 (80 m width). This narrowing concentrates the flow, thereby increasing the velocity. The upstream and downstream structures thus influence the flow conditions in the Verney widening, which cause its structuration. This phenomenon affects grain motion, at least at its boundaries, by ensuring favorable hydrodynamic conditions in a specific area.

5.2 Macroshape effects

The variation rate and standard deviation results show some local effects above the deposits at km 38.519. As shown in Fig. 2, the deposits on the right of the preferential channel consist of asymmetrical dunes. These macroshapes significantly influence the flow, especially the first meters of the water column (Best 2005). In Fig. 17, all the velocity profile shapes are similar with a local maximum close to the riverbed and a local minimum between 1 m and 1.5 m. Their

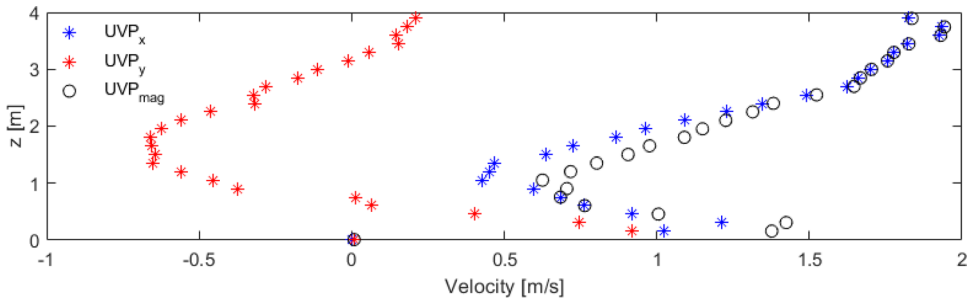

Fig. 17 Velocity profiles (streamwise, crosswise and magnitude-wise) at 55 m for the km 38.519 cross-section

similarity in height can be explained by their proximity to a 1 m high dune. These specific profiles correspond to the shear layers after the crest of a dune (de Cala et al. 2020). Unlike ripples, dunes interact with the full water column due to turbulent structures. The macroshapes thus explain the high variation rate and standard deviation observed previously for both cross-sections. The initial assumption of a logarithmic velocity profile cannot be respected near the dunes.

5.3 Scale and steady condition influence

An important note is that these dunes seem to be a model artifact. Indeed, sand is used to simulated bedload transport, i.e., gravel. Even if dunes can appear in gravel beds (Qin et al. 2015), it is more common to observe alternate bars (Nelson et al. 2009; Jaballah et al. 2015), which are expected for the future Rhone River (Canton of Valais). This difference in river morphology has a huge impact on the results. By upscaling, dunes are retained as well as all the phenomena related to them. Even if bedload transport similarity has been satisfied, only a length-distorted model can fulfil all modeling criteria of movable bed (Heller 2011) and maintain similarity with the river morphology. The steadiness of the system is also to be considered. Dunes last over time if hydraulic conditions are steady (Best 2005). However, discharges have not been changed in this case to determine the morphological time of the study perimeter. Without rapid changes, dunes would not disappear.

5.4 The preferential channel: area with conditions enabling grain motion

The Rhone River tends to return to its natural width despite the available space. Indeed, the width of the preferential channel is close to the width of the current channelized Rhone River. It was observed during the tests that the preferential channel occupies only a width of 50 to 60 m within the widening zone, although the widening zone is much larger. This value corresponds to its natural width (before the river training works), which ensures a large sediment transport capacity (Zarn 1997; Yalin and Da Silva 2001). This has been confirmed with the shear stress results. The hydraulic conditions in the preferential channel enable the grain motion. Indeed, the computed shear stresses are mainly higher than the critical shear stress for d_m. Therefore, fine particles ($d < d_m$) are likely to move. For larger particles ($d > d_m$), the motion conditions are achieved at isolated points. The calculated shear stress exceeds the critical shear stress for d_{90} only for four measurement locations. Based on these results, the preferential channel should be filled by the largest particles, which has not been observed.

Several explanations can be given. First, some grain sorting might occur upstream of the observed model reach, leaving some of the larger grains deposited upstream. The grain characteristics are the ones of the sediment introduced in the model. The grain mobility over distance is not considered. Secondly, Shield analysis considers only the interaction between the fluid driving forces and a grain. However, grain-grain interactions can be as significant (Leeder 1979; Frey and Church 2011) to the point of the formation of a grain-inertial flow (Hanes and Inman 1985a, b). According to Sumer and al. (Sumer et al. 1996), the velocity of the top of this sheet-flow layer follows the logarithmic law, while the rest follows a three-quarter power law. Some observations tend to confirm the assumption of a grain-inertial flow at the bottom of the preferential channel. Indeed, the bottom of some velocity profiles, especially in the preferential channel, seem to not follow the logarithmic flow, e.g. the one shown in Fig. 4 (2nd channel from the bottom).

According to Wilcock (1996), dimensionless shear stress between 0.03 and 0.06 already corresponds to partial transport therefore larger grains can be transported, especially within the already fully moving smaller particles. As shown in Table 5, most of the dimensionless shear stresses for d_{90} lie in this range. Moreover, the bathymetric survey shows insignificant changes in the preferential channel geometry during the measurement campaign with the bed in constant motion. This strengthens the idea that a sediment "conveyor belt" layer (Ferguson 1981; Kondolf 1997) at the bottom is formed, ensuring favourable conditions for the motion of larger grains. Visual observation confirms this assumption, but it needs to be further investigated.

6 Conclusions

In this paper, the grain motion potential of a larger river widening was assessed. Shear stress was calculated based on the logarithmic function between shear velocity and

Table 5 Mean dimensionless shear stress for d_m and d_{90} for UVP measurements located in the preferential channel for the cross-section at km 38.519

Measurement N°	23	22	21	20	19	18	17	16	15	14
$\tau_{cr,dm}$	0.013	0.100	0.033	0.044	0.084	0.214	0.127	0.060	0.065	0.209
$\tau_{cr,d90}$	0.006	0.044	0.014	0.020	0.037	0.095	0.056	0.027	0.029	0.093

the variation in velocity with height. Velocity profiles were acquired with a UVP allowing flow structures to be observed. Then, grain motion was assessed by comparing calculated shear stress with the critical shear stress. The results show a great potential for this method when hydraulic conditions suit its application (logarithmic velocity profile). From the assessment, the following items were observed:

- A structured flow is observed upstream and downstream of the widening with higher and steady velocities in the preferential channel compared to velocities above the deposits.
- Dunes strongly limit the application of the methodology presented in this paper. As shown, dunes are also moving, which indicates grain motion. However, these bedforms are retained while scaling up, even though they might not occur in reality. Moreover, the steadiness of the tests reinforces their presence.
- Shear stresses are higher in the preferential channel than the critical shear stresses for d_m and for d_{90} in most places along the preferential channel. This means bed particles are likely to move.
- Some grain sorting might occur upstream the observed model reach, leaving some of the larger grains deposited upstream.
- Dimensionless shear stress lower than the presumed critical value of 0.055 corresponds already to partial transport, therefore larger grains can be transported, especially within the already fully moving smaller particles.
- The bathymetric survey shows insignificant changes in the preferential channel geometry during the measurement campaign with the bed in constant motion. The main explanation is that a sediment "conveyor belt" layer at the bottom is formed, ensuring favorable conditions for the motion of larger grains.

Further experimental research on a lab setup must deal with improving the proposed methodology (turbulence measurements, turbulent kinetic energy method) (Biron et al. 2004) to apply it to more complex conditions, and to better assess the sediment transit in a large local river widening and how upstream and downstream structures affect the flow structure.

From the river engineering point of view regarding the Rhone River widening project, the decision has been taken to partially pre-excavate some morphologic structures in the future river widening such as the preferential channel, so that can act as a future bed load "conveyor belt" as previously portrayed by Kondolf (1997). The river is left to "do the rest" over time, with monitoring of the evolving bed morphology to prepare for potential corrective measures.

Acknowledgements The present study was supported by the *Canton of Valais, Rhone River flood protection service*. Our gratitude also goes to *Met-Flow* in Lausanne for their support of the use of the UVP instrument, and Meghan Irving for the English proofreading.

Authors' contributions All authors contributed to the study conception and design. Material preparation, data collection, and analysis were performed by Saugy Jean-Noël. The first draft of the manuscript was written by Saugy Jean-Noël and all authors commented on previous versions of the manuscript.

Funding Open access funding provided by EPFL Lausanne. Canton of Valais.

Availability of data and material Data available at Platform of Hydraulic Constructions, EPFL.

Code availability UVP Monitor version 3.0 (build 151) from Met-Flow, Cyclone version 2020.1.0 (Build 7697) from Leica Geosystem, 3DReshaper version 18.1.7.30029 from Hexagon, BASEMENT 2.8 from ETHZ and VAW, SMS version 13.0 from Aquaveo, and UVP_processing_v72 Matlab script (PL-LCH).

Declarations

Competing interests None.

Ethics approval Not applicable.

Consent to participate Yes.

Consent for publication Yes.

Open Access This article is licensed under a Creative Commons Attribution 4.0 International License, which permits use, sharing, adaptation, distribution and reproduction in any medium or format, as long as you give appropriate credit to the original author(s) and the source, provide a link to the Creative Commons licence, and indicate if changes were made. The images or other third party material in this article are included in the article's Creative Commons licence, unless indicated otherwise in a credit line to the material. If material is not included in the article's Creative Commons licence and your intended use is not permitted by statutory regulation or exceeds the permitted use, you will need to obtain permission directly from the copyright holder. To view a copy of this licence, visit http://creativecommons.org/licenses/by/4.0/.

References

Amini A, De Cesare G, Schleiss AJ (2009) Velocity profiles and interface instability in a two-phase fluid: investigations using ultrasonic velocity profiler. Exp Fluids 46:683–692. https://doi.org/10.1007/s00348-008-0594-1

Bagherimiyab F, Lemmin U (2013) Shear velocity estimates in rough-bed open-channel flow. Earth Surf Process Landf 38:1714–1724. https://doi.org/10.1002/esp.3421

Berchtold T, Vetsch DF, Weitbrecht V, Boes R (2012) Simulation of river-bed evolution due to channel widening. In: Proceedings of the 34th hydrology and water resources symposium, pp 299–307

Best J (2005) The fluid dynamics of river dunes: a review and some future research directions. J Geophys Res Earth Surf. https://doi.org/10.1029/2004JF000218

Bieri M, Müller M, Boillat J-L, Schleiss AJ (2012) Modeling of sediment management for the Lavey run-of-river HPP in Switzerland. J Hydraul Eng 138:340–347. https://doi.org/10.1061/(ASCE)HY.1943-7900.0000505

Biron P, Roy AG, Best JL (1996) Turbulent flow structure at concordant and discordant open-channel confluences. Exp Fluids 21:437–446. https://doi.org/10.1007/BF00189046

Biron PM, Robson C, Lapointe MF, Gaskin SJ (2004) Comparing different methods of bed shear stress estimates in simple and complex flow fields. Earth Surf Process Landf 29:1403–1415. https://doi.org/10.1002/esp.1111

Bohling B (2009) Measurements of threshold values for incipient motion of sediment particles with two different erosion devices. J Mar Syst 75:330–335. https://doi.org/10.1016/j.jmarsys.2007.01.014

Canton du Valais (2015) Plan d'aménagement (PA-R3). Canton du Valais, Service des routes, transports et cours d'eau, Section Protection contre les Crues du Rhône des services centraux

Canton du Valais (2020a) Carte des dangers hydrologiques. https://sitvalais.maps.arcgis.com/home/item.html?id=a3d6b35e28624caf8438d73f5a7291f5. Accessed 21 Oct 2021

Canton du Valais (2020b) Nature et paysage. https://www.vs.ch/web/rhone/nature-et-paysage. Accessed 17 Sept 2021

de Cala I, Ohata K, Dorrell R et al (2020) Relating the flow processes and bedforms of steady-state and waning density currents. Front Earth Sci 8:409. https://doi.org/10.3389/feart.2020.535743

De Cesare G, Boillat J-L (eds) (2006) Flow velocity measurements using ultrasound Doppler method—10 years experience in hydraulic modeling. In: Proceedings of international symposium on ultrasonic. Doppler methods for fluid mechanics and fluid engineering 12–14 Sept 2006

Duma D, Erpicum S, Archambeau P et al (2014) Flow and turbulence characterization as an onset for assessing the stability of gravel beds. In: Schleiss A, de Cesare G, Franca M, Pfister M (eds) River Flow 2014. CRC Press, Boca Raton, pp 891–898

Eawag, WSL, ETHZ, EPFL (2005) Local river widening. In: Integrales Gewässermanagement—Erkenn. Aus Dem Rhone-Thur Proj. https://www.wsl.ch/land/products/rhone-thur/en/river_wideni/rive_e.php. Accessed 11 Aug 2021

Essyad K, Magnollay A, Hunziker R et al (2014) Planifications stratégiques "Renaturation des Eaux" module charriage. Direction Générale de l'Environnement Division Ressources en eau et économie hydraulique

Ferguson R (1981) Channel form and channel changes. Br Rivers 90:125

Formann E, Habersack HM, St S (2007) Morphodynamic river processes and techniques for assessment of channel evolution in Alpine gravel bed rivers. Geomorphology 90:340–355. https://doi.org/10.1016/j.geomorph.2006.10.029

Franzetti S, Larcan E, Mignosa P (1982) Influence of tests duration on the evaluation of ultimate scour around circular piers. Papers presented at the international conference on the hydraulic modelling of civil engineering structures 1982, pp 381–396

Frey P, Church M (2011) Bedload: a granular phenomenon. Earth Surf Process Landf 36:58–69. https://doi.org/10.1002/esp.2103

Gaudio R, Miglio A, Calomino F (2010a) Friction factor and von Kármán's κ in narrow channels with bed-load. Mem E Studi 408

Gaudio R, Miglio A, Dey S (2010b) Non-universality of von Kármán's κ in fluvial streams. J Hydraul Res 48:658–663. https://doi.org/10.1080/00221686.2010.507338

Guney MS, Bombar G, Aksoy AO, Dogan M (2013) Use of UVP to investigate the evolution of bed configuration. KSCE J Civ Eng 17:1188–1197. https://doi.org/10.1007/s12205-013-0131-5

Hanes DM, Inman DL (1985a) Experimental evaluation of a dynamic yield criterion for granular fluid flows. J Geophys Res Solid Earth 90:3670–3674. https://doi.org/10.1029/JB090iB05p03670

Hanes DM, Inman DL (1985b) Observations of rapidly flowing granular-fluid materials. J Fluid Mech 150:357–380. https://doi.org/10.1017/S0022112085000167

Heller V (2011) Scale effects in physical hydraulic engineering models. J Hydraul Res 49:293–306. https://doi.org/10.1080/00221686.2011.578914

Hersberger D (ed) (2002) Measurement of 3D flow field in a 90° bend with ultrasonic Doppler velocity profiler. In: Proceedings of third international symposium on ultrasonic Doppler methods for fluid mechanics and fluid engineering EPFL Lausanne Switz

Hinkelammert F, Friedl F, Weitbrecht V (2016) Sohlaufnahme durch bewegte Wasseroberfläche mittels Laserscanning. In: Wasserbau - mehr als Bauen im Wasser : Beiträge zum 18. Gemeinschafts-Symposium der Wasserbau-Institute TU München, TU Graz und ETH Zürich vom 29. Juni bis 1. Juli 2016 in Wallgau, Oberbayern. TUM, Technische Universität München, Lehrstuhl für Wasserbau und Wasserwirtschaft, pp 195–204

Hjulström F (1935) Studies of the morphological activity of rivers as illustrated by the River Fyris. Almqvist & Wiksell., Uppsala

Horn BKP, Schunck BG (1981) Determining optical flow. Artif Intell 17:185–203. https://doi.org/10.1016/0004-3702(81)90024-2

Hunzinger LM (1998) Flussaufweitungen: Morphologie, Geschiebehaushalt und Grundsätze zur Bemessung. Doctoral Thesis, ETH Zurich

Inman DL (1949) Sorting of sediments in the light of fluid mechanics. J Sediment Res 19:51–70. https://doi.org/10.1306/D426934B-2B26-11D7-8648000102C1865D

Jaballah M, Camenen B, Pénard L, Paquier A (2015) Alternate bar development in an alpine river following engineering works. Adv Water Resour 81:103–113. https://doi.org/10.1016/j.advwatres.2015.03.003

Jenzer J, Pereira SC, Federspiel M, Boillat J-L (2008) Multi-purpose modelling of the Rhone River in the region of Visp (Switzerland). In: Conference proceeding INTERPRAEVENT 2008, vol 1, p a9

Kantoush SA, De Cesare G, Boillat JL, Schleiss AJ (2008) Flow field investigation in a rectangular shallow reservoir using UVP, LSPIV and numerical modelling. Flow Meas Instrum 19:139–144. https://doi.org/10.1016/j.flowmeasinst.2007.09.005

Kondolf G (1997) PROFILE: hungry water: effects of dams and gravel mining on river channels. Environ Manag 21:533–551. https://doi.org/10.1007/s002679900048

Lane EW (1955) Design of stable channels. Trans Am Soc Civ Eng 120:1234–1260. https://doi.org/10.1061/TACEAT.0007188

Leeder MR (1979) 'Bedload' dynamics: grain–grain interactions in water flows. Earth Surf Process 4:229–240. https://doi.org/10.1002/esp.3290040304

Matt J (2021) Absolute orientation—Horn's method. https://ch.mathworks.com/matlabcentral/fileexchange/26186-absolute-orientation-horn-s-method. Accessed 11 Aug 2021

Meile T, De Cesare G, Blanckaert K, Schleiss AJ (2008) Improvement of acoustic Doppler velocimetry in steady and unsteady turbulent open-channel flows by means of seeding with hydrogen bubbles. Flow Meas Instrum 19:215–221. https://doi.org/10.1016/j.flowmeasinst.2007.08.009

Metflow (2002) UVP monitor model UVP-DUO—users guide. Metflow SA, Lausanne, Switzerland

Muste M, Fujita I, Kruger A (1998) Experimental comparison of two laser-based velocimeters for flows with alluvial sand. Exp Fluids 24:273–284. https://doi.org/10.1007/s003480050174

Nelson PA, Venditti JG, Dietrich WE et al (2009) Response of bed surface patchiness to reductions in sediment supply. J Geophys Res Earth Surf. https://doi.org/10.1029/2008JF001144

Nilipour N, De Cesare G, Boillat J-L (eds) (2004) Application of UVP transducers to measure bed geometry and velocity profiles in a hydraulic scale model with gravel pit. In: Proceedings of 4th

international symposium on ultrasonic Doppler method for fluid mechanics and fluid engineering 4th ISUD

Paphitis D (2001) Sediment movement under unidirectional flows: an assessment of empirical threshold curves. Coast Eng 43:227–245. https://doi.org/10.1016/S0378-3839(01)00015-1

Pilotti M, Menduni G, Castelli E (1997) Monitoring the inception of sediment transport by image processing techniques. Exp Fluids 23:202–208. https://doi.org/10.1007/s003480050103

Qin J, Wu T, Zhong D (2015) Spectral behavior of gravel dunes. Geomorphology 231:331–342. https://doi.org/10.1016/j.geomorph.2014.12.023

Radice A, Malavasi S, Ballio F (2006) Solid transport measurements through image processing. Exp Fluids 41:721–734. https://doi.org/10.1007/s00348-006-0195-9

Rohde S, Schütz M, Kienast F, Englmaier P (2005) River widening: an approach to restoring riparian habitats and plant species. River Res Appl 21:1075–1094. https://doi.org/10.1002/rra.870

Rosier B, Jordan F, De Cesare G et al (eds) (2004) Determination of velocity profiles and bed morphology using UVP transducers to investigate the influence of lateral overflow on mobile bed. In: Proceedings of 4th international symposium on ultrasonic Doppler method for fluid mechanics and fluid engineering 4TH ISUD

Schirmer M, Luster J, Linde N et al (2014) Morphological, hydrological, biogeochemical and ecological changes and challenges in river restoration—the Thur River case study. Hydrol Earth Syst Sci 18:2449–2462. https://doi.org/10.5194/hess-18-2449-2014

Schlichting H, Gersten K, Krause E, Oertel HJ (1979) Boundary-layer theory, 7th edn. McGraw-Hill, New York

Shields A (1936) Anwendung der Aehnlichkeitsmechanik und der Turbulenzforschung auf die Geschiebebewegung. PhD Thesis Tech Univ Berl

Sumer BM, Kozakiewicz A, Fredsøe J, Deigaard R (1996) Velocity and concentration profiles in sheet-flow layer of movable bed. J Hydraul Eng 122:549–558. https://doi.org/10.1061/(ASCE)0733-9429(1996)122:10(549)

Sundborg Å (1956) The river Klarälven a study of fluvial processes. Geogr Ann 38:125–316. https://doi.org/10.1080/20014422.1956.11880887

Takeda Y (1986) Velocity profile measurement by ultrasound Doppler shift method. Int J Heat Fluid Flow 7:313–318. https://doi.org/10.1016/0142-727X(86)90011-1

Takeda Y (1991) Development of an ultrasound velocity profile monitor. Nucl Eng Des 126:277–284. https://doi.org/10.1016/0029-5493(91)90117-Z

Tal M, Frey P, Kim W et al (2012) The use of imagery in laboratory experiments. In: Fluvial remote sensing for science and management. Wiley, pp 299–321. https://doi.org/10.1002/9781119940791.ch13

Van Rijn CL (1984) Sediment transport, part I: bed load transport. J Hydraul Eng 110:1431–1456. https://doi.org/10.1061/(ASCE)0733-9429(1984)110:10(1431)

Von Kármán T (1930) Mechanische Ähnlichkeit and Turbulenz. Nachrichten Adademie Wiss Gött Mathematisch-Physikalische Klasse 1:58–76

Wang XY, Yang QY, Lu WZ, Wang XK (2012) Experimental study of near-wall turbulent characteristics in an open-channel with gravel bed using an acoustic Doppler velocimeter. Exp Fluids 52:85–94. https://doi.org/10.1007/s00348-011-1202-3

Weber C, Schager E, Peter A (2009) Habitat diversity and fish assemblage structure in local river widenings: a case study on a swiss river. River Res Appl 25:687–701. https://doi.org/10.1002/rra.1176

Wilcock PR (1996) Estimating local bed shear stress from velocity observations. Water Resour Res 32:3361–3366. https://doi.org/10.1029/96WR02277

Worley FL (1972) Statistical fluid mechanics. Monin AS, Yaglom AM M.I.T. Press, Cambridge, MA (1971). $18.50. AIChE J 18:1087–1087. https://doi.org/10.1002/aic.690180546

Yalin MS (1971) Theory of Hydraulic Models. Macmillan Education UK, London

Yalin MS, Da Silva AF (2001) Fluvial processes. IAHR, Delft

Yamanaka G, Kikura H, Takeda Y, Aritomi M (2002) Flow measurement on an oscillating pipe flow near the entrance using the UVP method. Exp Fluids 32:212–220. https://doi.org/10.1007/s003480100367

Zarn B (1997) Einfluss der Flussbettbreite auf die Wechselwirkung zwischen Abfluss, Morphologie und Geschiebetransportkapazität. ETH Zurich

Publisher's Note Springer Nature remains neutral with regard to jurisdictional claims in published maps and institutional affiliations.